ACS Catalysis

Perspective

pubs.acs.org/acscatalysis

In Situ Surface and Reaction Probe Studies with Model Nanoparticle Catalysts

Selim Alayoglu,[†,‡] James M. Krier,[†,‡] William D. Michalak,[†,‡] Zhongwei Zhu,[†,§] Elad Gross,[†,‡] and Gabor A. Somorjai*[,†,‡,§]

[†]Department of Chemistry, University of California, Hildebrand Hall, Berkeley, California 94720, United States

[‡]Chemical Sciences Division and [§]Materials Sciences Division, Lawrence Berkeley National Laboratory, 1 Cyclotron road, Berkeley,California 94720, United States

ABSTRACT: This review paper discusses the in situ surface characterization and catalytic measurements of colloidally synthesized model metal nanoparticle (NP) catalysts studied in the Somorjai lab. Sum Frequency Generation (SFG) vibrational spectroscopy technique revealed the vibrational signatures of binding geometry and surface orientation of adsorbate molecules by probing the immediate surface structure during the catalytic reactions. Metal surfaces were studied by Synchrotron-based spectroscopic techniques at the Advanced Light Source in the Lawrence Berkeley National Laboratory. Ambient Pressure X-ray Photoelectron Spectroscopy (APXPS) was employed to measure chemical and elemental structure of bimetallic NP catalysts under the catalytically relevant pressures in the Torr range. Surface chemical structure (i.e., oxidation states) of metals was obtained by X-ray Absorption Fine Structure Spectroscopy by constructing a gas flow cell that operates under atmospheric pressures as the reaction occurs. Environmental Transmission Electron Microscopy (E-TEM) supplemented the bimetallic structure that was obtained by X-ray spectroscopies. The morphology and chemistry induced by gas reactants on the stepped single crystal surfaces as determined by high-pressure in situ Scanning Tunneling Microscopy (HPSTM) and APXPS were also described.

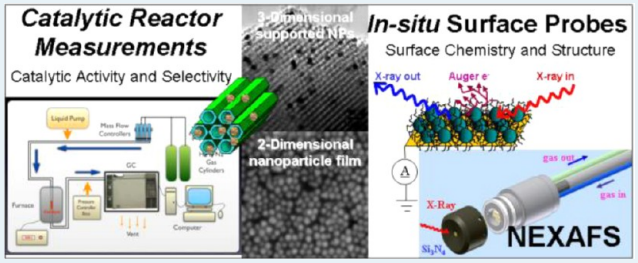

KEYWORDS: *colloidal nanoparticle catalysts, in situ surface probes, surface sum frequency generation vibrational spectroscopy, ambient pressure x-ray photoelectron spectroscopy, near edge x-ray absorption fine structure, oxidation states, elemental composition, catalytic reactivity measurements*

INTRODUCTION

In heterogeneous catalysis, metal and/or metal oxide particles with sizes usually in the nanoscale are employed to catalyze reactions in the gas or liquid phases. These nanoparticle (NP) catalysts are now synthesized using colloidal routes with an atomic level control of the particle size and architecture, crystallographic orientation, morphologic shape, and elemental and chemical composition on the surface and in the bulk.[1,2] It has been demonstrated that the surfaces of colloidally fabricated NPs are dynamic and change under the reactive gas atmospheres.[3−5] In many respects, this behavior is similar to observations from single crystal surfaces.[6,7] Hence, in situ and operando studies in catalysis are essential for a thorough understanding of catalytic processes and the relationships between NP surface structure and reactivity.[8,9]

Over the past 15 years, our group has contributed to the fundamental understanding of catalytic reactivity of colloidal NPs at the molecular level. Systematic and comprehensive studies have identified seven molecular factors that impact catalytic properties. These include reaction intermediates, reactant mobility, particle size, composition, crystallographic shape, oxidation state, and metal−support interaction.

The available experimental results indicate that surfaces undergo chemical and structural changes during catalytic reactions. As a result, pre- and post-catalytic characterization provides little molecular insight into the mechanistic, dynamic, and kinetic aspects of catalytic processes. Hence, the use of in situ surface techniques is of fundamental importance in the development of a corroborating and unifying picture of surface chemistry and catalysis.

A. In Situ Tools of Surface Chemistry and Catalysis.

1. Surface Sum Frequency Generation Vibrational Spectroscopy (SFGVS) for Studying Metal-Adsorbate Bonding and Orientation. Surface ensemble and surface composition are essential to the fundamental understanding of surface reactivity of mono- and multicomponent metal NP catalysts. Polarization modulation infrared reflectance vibrational spectroscopy[10] and Sum Frequency Generation (SFG) vibrational spectroscopy[11]

Special Issue: Operando and In Situ Studies of Catalysis

Received: July 20, 2012
Revised: September 19, 2012
Published: September 21, 2012

are surface-sensitive techniques that can be used to probe the ensemble of surface atoms.[12−18]

SFG allows organic species on the surface of catalysts to be monitored under catalytically relevant operating conditions.[19,20] In a typical experiment (Figure 1), infrared and visible beams

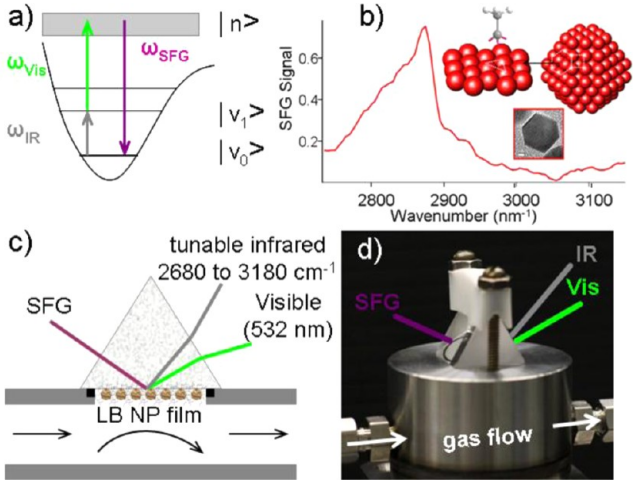

Figure 1. (a) Energetic excitation diagram for sum frequency generation. (b) Representative SFG vibrational spectrum of ethylene hydrogenation on cubooctahedral Pt NPs. The peak at 2870 cm^{-1} indicates ethylidyne. (c) Experimental schematic and (d) picture of SFGVS flow reactor setup.

with 20 ps pulse widths are spatially and temporally overlapped as the reactant adsorbs onto the sample. Information gained with SFG, like the presence of methyl and methylene vibrational bands, is often comparable to other forms of vibrational spectroscopy (including infrared and Raman). However, SFG is entirely interface selective, which makes it ideal for studying catalysis (Figure 1b). Because SFG is a coherent second order optical process, only vibrational modes with a net orientation perpendicular to the surface will produce signal. Disordered vibrations, which often appear in bulk media, cancel and do not contribute to the SFG signal. SFG spectra also reflect how organic molecules arrange on the surface because the relative contribution of symmetric and asymmetric stretches change based on the geometry of the adsorbate. For example, the relative intensities of $CH_2(s)/CH_2(a)$ and $CH_3(s)/CH_3(a)$ were used previously to determine whether adsorbed hexyl species were lying flat or standing upright on Pt(111).[21]

2. Ambient Pressure X-ray Photoelectron Spectroscopy (APXPS) for Evaluating Chemical Composition and Oxidation States. Photoelectron spectroscopies featuring the energy tunable high flux of synchrotron radiation and the short mean free paths (in the order of nanometers) of electrons in a solid provide the necessary tools for studying surface chemical composition and oxidation states of NP catalysts (Figures 2a and 2b). X-ray Photoelectron Spectroscopy (XPS), which is conventionally an ultrahigh vacuum technique, can be used with ambient reactive gases in the low Torr pressure regime by using a differentially pumped stage that separates the gas atmosphere from the electron energy analyzer (e.g., Beamline 9.3.2 at the Advanced Light Source (ALS) at the Lawrence Berkeley National Laboratory (Figure 2c)).[22,23] With this configuration, elemental composition and redox states of the surface and subsurface regions of NP catalyst regions can be

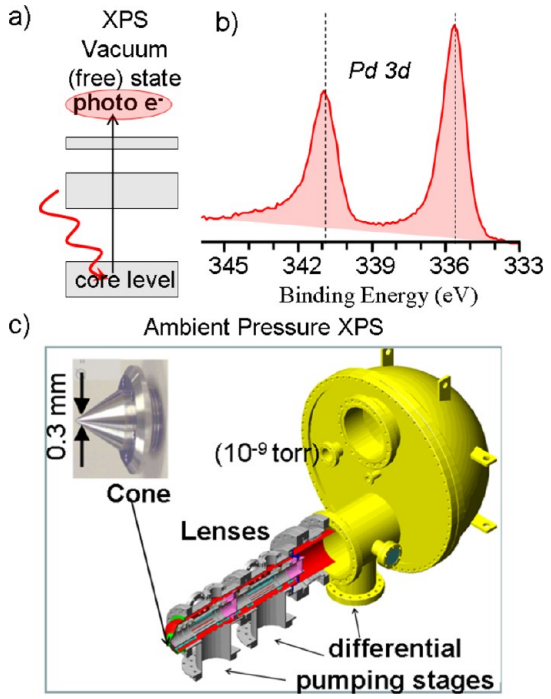

Figure 2. (a) X-ray induced photoelectron (XP) ejection of core level electrons into vacuum can be used to identify the chemical composition of a material. Representative XP spectrum at the Pd 3d core levels of bimetallic PdRh nanoparticles under CO oxidation reaction and (b) at 200 °C. (c) Schematic of ambient pressure XPS setup at the Beamline 9.3.2 of the Advanced Light Source at the Lawrence Berkeley National Laboratory.

evaluated under catalytically relevant reaction pressures. Using this tool, reaction kinetics can be correlated to surface composition and oxidation states under catalytically relevant atmospheres.

3. In Situ near Edge X-ray Absorption Fine Structure (NEXAFS) Spectroscopy for Investigating Oxidation States. Synchrotron-based X-ray Absorption Spectroscopy (XAS) also features the means to study the near surface regions of NP catalysts under atmospheric pressures and at elevated temperatures. Near Edge X-ray Absorption Fine Structure (NEXAFS) spectroscopy informs about the oxidation states of transition metals by detecting X-ray fluorescence from electron relaxation following the core level electron excitation and/or electrons compensating emitted Auger electrons (Figure 3a). In the latter case, the electron flow from electrical ground is measured; this is unlike detection in X-ray photoelectron spectroscopy (XPS) in which free photoelectrons are detected in vacuum. NEXAFS spectroscopy measures the immediate vicinity (10−50 eV) of the absorption edge and gives element specific chemical information. The technique is very sensitive to oxidation states for the L-edge absorption of the first and second row transition metals using soft X-rays (400−3000 eV).[24,25] Soft X-ray based NEXAFS is surface sensitive in the electron detection mode with probing depths in the order of a few nanometers, (~2 nm for first row transition metals like Co);[26] whereas, fluorescence detection is limited to the penetration depth of absorbed X-rays (typically about 300 nm with soft X-rays). On the other hand, X-ray cross sections are larger with electron yield signals compared to the fluorescence yield signals for the L-edge absorption of first row transition metals, as shown for Co L-edge in Figure 3b. Fluorescence yield becomes surface sensitive

dx.doi.org/10.1021/cs3004903 | ACS Catal. 2012, 2, 2250−2258

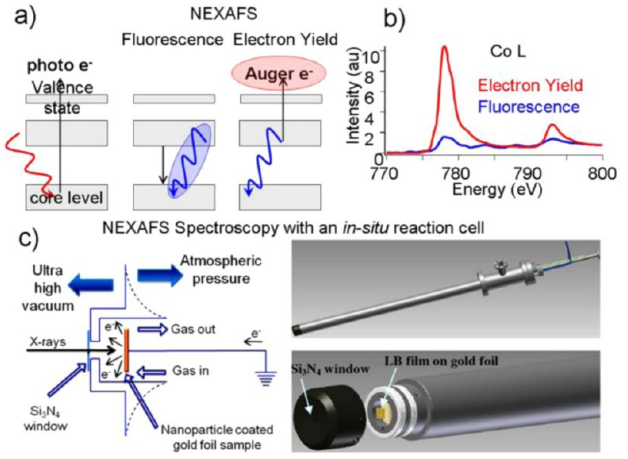

Figure 3. (a) Depictions of X-ray absorption inducing core level electron excitation using near edge X-ray absorption fine structure (NEXAFS) spectroscopy. (b) Representative NEXAFS spectra (electron yield and fluorescence) at the Co L edge of pure Co nanoparticles under 1 atm H_2 and at 200 °C. (c) Schematics of in situ gas flow cell purposely built for NEXAFS at the beamline 7.0.1 at the Advanced Light Source (reprinted with permission from ref 68, copyright 2011 American Chemical Society).

for small and ultrasmall NPs where the bulk to surface ratio approaches one.[27] Thus, both the surface and the bulk of transition metal NPs can be simultaneously monitored with NEXAFS spectroscopy in the soft X-rays regime.

NEXAFS spectroscopy using soft X-rays is limited to gas pressures of a few bars above atmospheric owing to signal attenuation by absorption in the gas phase (as depicted by the picture in Figure 3c). Furthermore, XAS requires an in situ reaction cell with X-ray permeable thin membranes; typically 100−200 nm thick Si_3N_4 for soft X-rays and 1 μm thick Si_3N_4 windows (or quartz, Kapton, Mylar or Be) for hard X-rays to hold against the large differential pressures.

4. Environmental and in Situ Transmission Electron Microscopy (E-TEM) for Composition and Morphology Analysis. Electron microscopy techniques employing an in situ reaction holder[28] or environmental cell[29] uniquely provide the dynamics concerning the particle size, shape and morphology at the single particle level under static or flowing reactive gas pressures.[30] Z-contrast imaging obtained by the annular dark field technique in the scanning mode and/or diffraction imaging in the transmission mode can distinguish between the metal components of an alloy NP and thus help to map out elemental composition across a single particle under reaction conditions.

This review paper focuses on the in situ characterization of colloidal NP films and supported catalysts coupled to the catalytic measurements reported recently from our lab. In the first part, in situ reaction and surface probe studies employing SFG will be discussed. The second part will discuss the in situ elemental and chemical composition analysis of NP catalysts employing Synchrotron-based spectroscopic techniques and Environmental Transmission Electron Microscopy (E-TEM). Also in the second part, the break-up of Pt(557) stepped crystal surface and the oxidation of Pt(110) crystal surface induced by redox gases in Torr pressure regimes will be described and discussed in relation to what is expected for the behavior of colloidal metal NPs.

B. Nature of Surface Metal-Adsorbate Interactions of Colloidal Metal NPs. Beginning in the mid-1990s we initiated SFG studies to monitor processes on catalytic surfaces. Early work focused exclusively on perfect single crystals including Pt(111), Pt(100), and Rh(111), and model reactions like CO adsorption,[31] ethylene hydrogenation[32] and cyclohexene hydrogenation.[33] The cyclohexene hydrogenation reaction is particularly well suited for SFG studies because the three most common chemisorbed intermediates, 1,4-cyclohexadiene, 1,3-cyclohexadiene, and the π-allyl geometry of cyclohexene, can be distinguished from one another in the range of aliphatic vibrations (2700−3000 cm^{-1}). For this reason, the adsorption and hydrogenation of cyclohexene is very well documented by SFG on Pt single crystals.[33−37]

1. Reaction Intermediates Studied by SFGVS. More recently, our focus has shifted from single crystals to size- and shape-controlled NPs made by colloidal synthesis methodologies.[38] Already, several studies have documented the impact of size on reaction selectivity in the range of 1−5 nm Pt.[39,40] However, a major hurdle presented by colloidal particles is the organic capping agent. The experimental protocols developed to clean single crystals, such as sputtering and annealing, cannot be applied to NPs because the treatments destroy the cap and cause sintering of the NPs. With untreated NPs, strong features from the organic capping mask the features of the reactive intermediates in the SFG spectra. Cap removal with UV light was proposed as a way to reduce the SFG signal from the capping agent. Using this method, reactive intermediates of dimethyl and methyl furan were identified on 7 nm Pt cubes and correlated to reaction selectivity.[41]

Across the temperature range of 40−120 °C, cracking products (alcohols) dominated with respect to tetra- and dihydrofuranic species for both dimethyl and methyl furan hydrogenation. SFG spectra with the proposed reaction intermediates are shown in Figure 4. The appearance of symmetric and asymmetric CH_2/CH_3 peaks in the spectra suggests that the reaction intermediates have their O bound to Pt, which corroborates the selectivity preference for cracking at high temperatures (C−O bond scission). For dimethyl furan, uncracked hydrogenation products (dihydrodimethyl furan and tetrahydrodimethyl furan) are observed at lower temperatures, and the ring-structure is expected to be lying parallel to the surface.

2. Removal/Disordering of Organic Capping Agent Studied by SFGVS. UV cleaning effectively removes PVP and increases available active sites by a factor of 10.[42] However, UV cleaning to study NPs with SFG has two limitations. First, Pt-PVP NPs are considerably more prone to aggregation under reaction conditions once PVP is removed. Second, residual C fragments persist even after long UV treatments.[43] Residual fragments of PVP can impact reaction pathways. This was observed for cyclohexene hydrogenation on 4 nm Pt-PVP (Figure 5c). Following UV treatment, two intermediates (1,3-cyclohexadiene and the π-allyl geometry of cyclohexene) are observed, while they are not observed on lightly UV treated Pt-PVP or on the Pt(111) single crystal treated with similar reaction conditions.[36]

Recent work has shown that signal associated with PVP can be removed from the SFG spectra through molecular disordering via H_2 as opposed to complete cap removal.[42] Figure 5a shows 4 nm Pt-PVP under Ar (top) and then under 200 Torr of H_2 (bottom). Under H_2, there is a ∼90% decrease in signal that originates from PVP. The disordering/molecular

dx.doi.org/10.1021/cs3004903 | ACS Catal. 2012, 2, 2250−2258

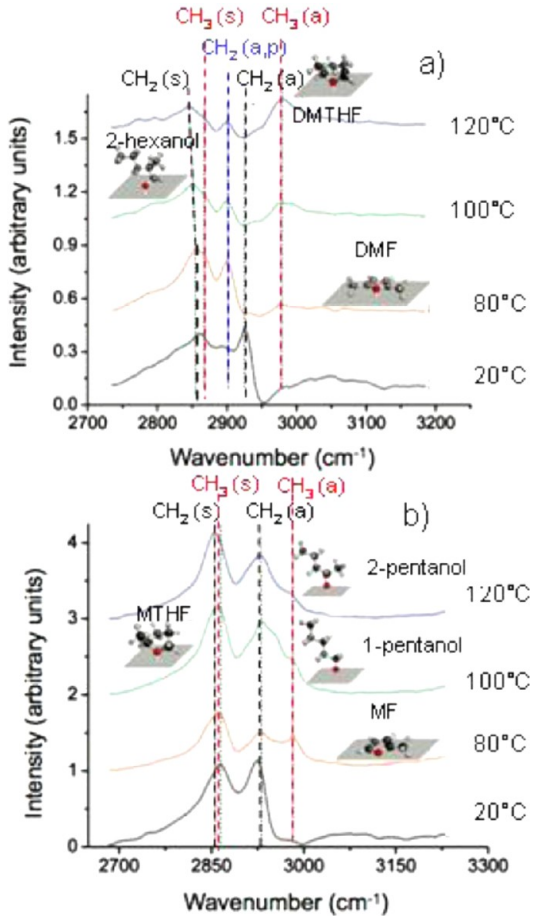

Figure 4. (a) Methyl furan hydrogenation and (b) dimethyl furan hydrogenation on 7 nm Pt-PVP cubes following UV cleaning. A reaction mixture of 10/100 Torr (di)methyl furan/H_2 with Ar fill was used for all experiments (reprinted with permission from ref 41, copyright 2011 American Chemical Society).

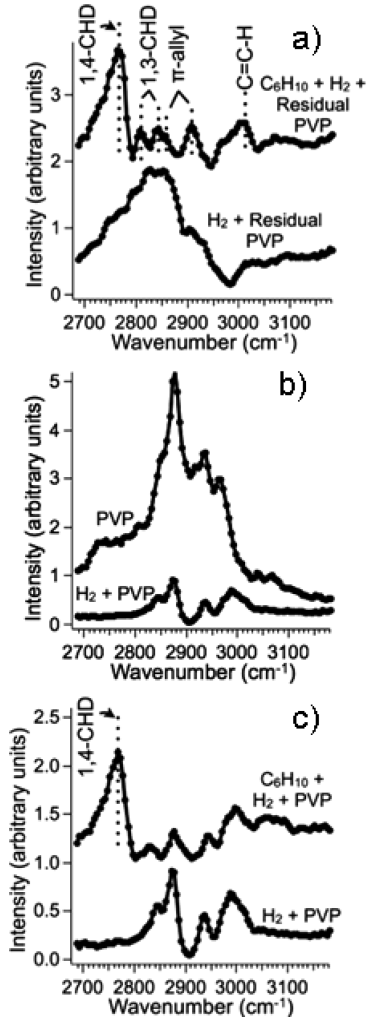

Figure 5. (a) 4 nm Pt-PVP exposed to 760 Torr Ar (top) and 200 Torr H_2 with 560 Torr Ar (bottom). (b) 4 nm Pt-PVP exposed first to 200 Torr H_2 with 560 Torr Ar (bottom) then to 10 Torr cyclohexene (C_6H_{10}) with 200 Torr H_2 and 560 Torr Ar (top). (c) 4 nm Pt-PVP following 180 min UV cleaning exposed to identical conditions as (b) (reprinted with permission from ref 42, copyright 2012 American Chemical Society).

reorientation effect was found to be reversible, and the 1,4-cyclohexadiene intermediate observed on Pt(111) was also identified on PVP capped 4 nm Pt NPs.[36] In addition, since PVP is left intact, the particles are stable under most hydrogenation reaction conditions (up to at least 200 °C). Performing SFG with PVP intact is particularly advantageous because most size-controlled kinetic studies of Pt-PVP particles do not use aggressive cap removal.[44−46] In this way, SFG can be used to correlate the selectivity changes with changes in the reactive intermediates.

C. Reaction-Induced Surface Dynamics and the Impact on Catalysis. The oxidation state of a catalyst has a critical role over the activity and selectivity to various products in catalytic reactions.[27,47−49] Both theoretical and experimental studies over the past decade have shown that the oxidation state of an active catalyst can vary by introducing reducing or oxidizing environments or even because of the presence of another metal. The addition of another metal may impact the number of nearest neighbor metal atoms, the electronic state of the metal,[50,51] and the particle size and morphology.[52−58] Variations in these properties cause catalysts to have different susceptibilities for oxidation and reduction. Since the oxidation state is sensitive to the chemical environment and reaction temperature and pressure, understanding the properties of catalysts using in situ or operando methods is imperative for understanding catalysts operating under reaction conditions.

1. Monometallic Systems. (a). In Situ NEXAFS Spectroscopy Study of Heterogeneous Catalysts in a Homogeneous Environment. The correlation between the oxidation state of metallic NPs and their catalytic reactivity toward homogeneous reactions in the liquid phase were studied by XAS at beamline 10.3.2 at the ALS.[59] We found that by controlling and modifying the oxidation state of 40 metal atom, dendrimer-encapsulated, Pt and Pd clusters with a diameter of ∼1 nm, the metallic clusters can be activated toward electrophilic hydroalkoxylation reactions (Figure 6).[59,60] Dendrimer encapsulated metallic NPs loaded on mesoporous silica supports showed high catalytic reactivity, following oxidation by $PhICl_2$, for a variety of π-bond activated reactions that were previously known to be solely catalyzed by homogeneous catalysts.

While no catalytic reactivity was obtained when using the reduced dendrimer-encapsulated metallic NPs, high reactivity was measured when the metallic NPs were oxidized by an organic oxidizer, $PhICl_2$, using toluene as a solvent. To

dx.doi.org/10.1021/cs3004903 | ACS Catal. 2012, 2, 2250−2258

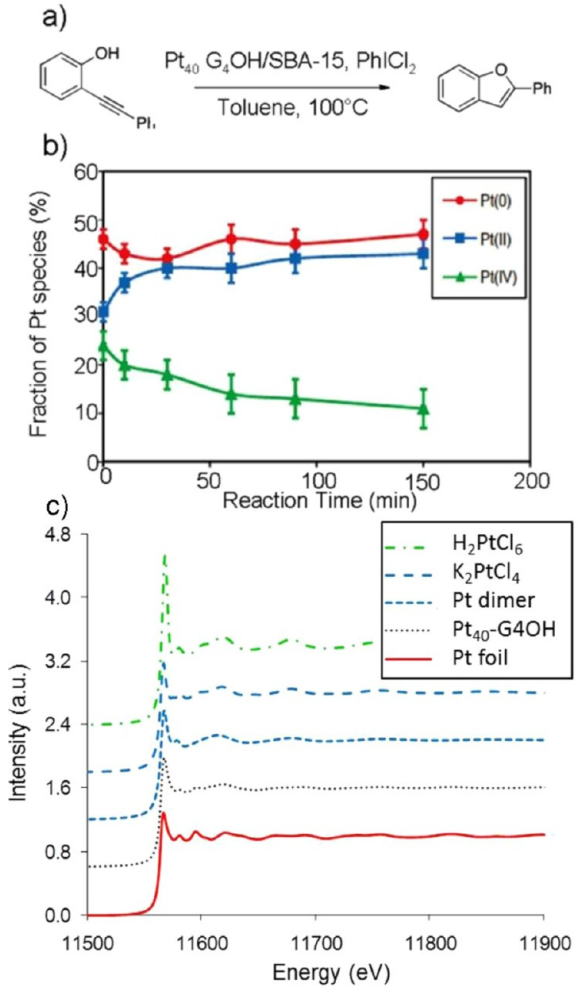

Figure 6. (a) Reaction scheme for the electrophilic hydroxylation over ~1 nm dendrimer-capped Pt NPs. (b) Percentage of Pt species obtained in situ using quick NEXAFS and (c) NEXAFS spectra of the sample dendrimer-capped Pt NPs and various reference standards used for the least-squares fitting procedure in (b) (reprinted with permission from ref 59, copyright 2011 American Chemical Society).

elucidate the true nature of the active catalyst, the supported dendrimer-encapsulated Pt NPs were studied with in situ NEXAFS spectroscopy. NEXAFS analysis indicated that about 25% of the Pt atoms in the catalytically active, oxidized clusters were Pt(IV) and about 50% of the Pt atoms stayed in their reduced state, Pt(0) (Figure 6b). During the course of reaction with ~70% completion, metallic Pt(0) remained at about 50% whereas the percentage of Pt(IV) went to 10% at the expense of Pt(II) formation. For a control experiment, no Pt(IV) species was detected ex situ following the reduction of the supported catalyst by exposure to H_2. Furthermore, the reduced catalyst was found inactive toward the π-activation reaction, which indicated that the Pt(IV) species were the catalytically active species in this system.

The coordination number of the Pt atoms under reduced and oxidized conditions was analyzed by ex situ EXAFS measurements. Oxidation of the catalyst, using $PhICl_2$ as an oxidizer, led to a decrease in the Pt−Pt coordination number from five to one; whereas, the coordination number of Pt−Cl was increased from zero to two. These results indicate fragmentation of Pt clusters and that the highly oxidized Pt was coordinated to the negatively charged Cl^- ions.

The XAS results indicate that the active species for π-activation reactions in dendrimer encapsulated Pt NPs is the Pt(IV) species, stabilized by Cl^- ions. By repeating the reduction and oxidation procedure, the percentage of highly oxidized Pt(IV) and the coordination number of Pt−Cl were increased concomitantly with the reaction rate. The reversibility of the oxidation−reduction cycles demonstrates the stability of the heterogeneous dendrimer-encapsulated Pt NP catalyst under different conditions. The demonstrated behavior also excludes the possibility of any leaching of metal ions to the solution phase following the oxidation−reduction cycles.

(b). APXPS Study of Size Effect of Rh NPs for CO Oxidation. The particle size of nanoparticle catalysts has been shown to have a dominant effect on catalytic activity. For example, in CO oxidation small Pd particles are most active,[53] whereas the opposite was true for Pt.[7] In our lab, we studied the size effect for Rh catalysts in CO oxidation.[61] At a constant temperature of 200 °C, the turnover frequency (TOF) to CO_2 increases 5-fold as the particle diameter decreases from 11 to 2 nm with a reduction in the activation barrier from 27.9 to 10 kcal/mol. To understand the role of the oxidation state of Rh, we used in situ APXPS at Beamline 11.0.2 at the ALS. Following initial oxidation at 200 °C, the high binding shoulders at 308.2 and 309.4 eV of the Rh $3d_{5/2}$ peak indicated that the 2 nm particles were more oxidized with 70% Rh^{3+} compared to the 7 nm particles with 54% Rh^{3+}. Following the oxidation treatments, the samples were monitored at 150 and 200 °C with 200 mTorr of CO and 500 mTorr O_2 (Figure 7).

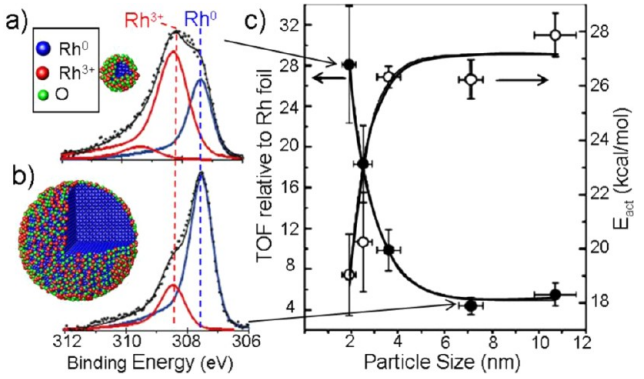

Figure 7. Representative APXPS Rh 3d spectra of (a) 2 nm and (b) 7 nm Rh NP films under 200 mTorr CO with 500 mTorr O_2 at 200 °C. (c) Turnover rates relative to Rh foil (left axis), and the activation energies (right axis) as a function of particle sizes in the 2−11 nm range over the Rh NP films (reprinted with permission from ref 61, copyright 2008 John Wiley and Sons).

Both samples were reduced under reactions conditions and exhibited 67% Rh^{3+} and 25% Rh^{3+} for the 2 and 7 nm particles, respectively. During CO oxidation, the O 1s peak was also monitored. A low binding energy peak at 529.5 eV was observed under reaction conditions, while the shoulder was not observed when heating in O_2. This suggests that a distinct "reactive oxide" is stabilized by CO or another reaction intermediate. This stable reactive oxide on the 2 nm particles is believed to be the active site that contributes to the 5-fold enhancement of the TOF.

(c). HPSTM Study of Break-up and Clustering of Pt(557) Stepped Crystal Surfaces. Not only does the presence of gas reactants alter the oxidation states of catalyst surface species, the morphology of catalyst surfaces also undergo significant

dx.doi.org/10.1021/cs3004903 | ACS Catal. 2012, 2, 2250−2258

changes as a result of adsorbate−substrate interaction. Scanning tunneling microscopy (STM) has advanced the exploration of the local electronic and morphologic structure changes of catalysts owing to the technique's distinct capability of imaging surfaces at the nanometer scale. With the development of high-pressure STM, our group has been investigating the catalyst surface structures under ambient conditions for almost two decades.[62,63]

Recently we have focused on the structural changes of stepped single crystal surfaces as a model for catalysts in high-pressure STM experiments. Stepped metal single crystals are able to mimic the real NP catalysts because of the high concentration of low-coordinated step sites on the surfaces. The Pt(557) consists of terraces with 6 rows of (111)-type sites and monatomic (100)-type steps, with the average terrace width being 1.4 nm between steps (Figure 8). When the

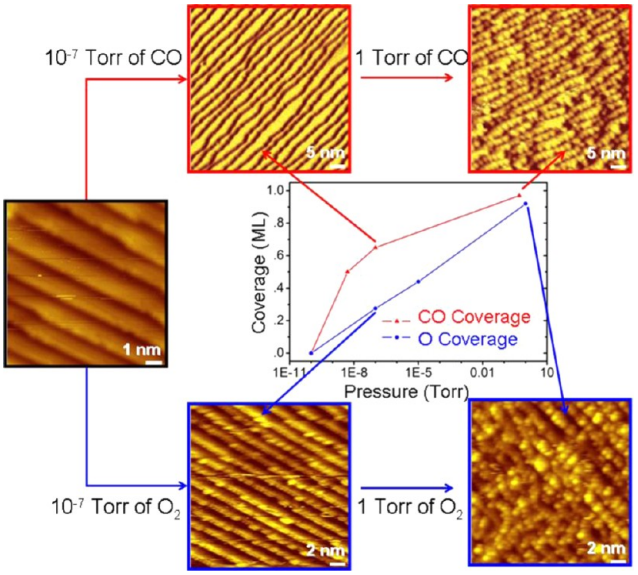

Figure 8. STM pictures of the stepped Pt(557) single crystal surfaces under UHV and various CO (or O_2) partial pressures. A plot of surface coverage, derived from AP-XPS Pt 4f and C 1s (or O 1s) spectra, is shown as a function of CO (or O_2) partial pressure (reprinted with permissions from ref 64, copyright 2010 American Association for the Advancement of Science; and ref 65, copyright 2012 American Chemical Society).

Pt(557) was exposed to 1 Torr of CO, the steps rearranged into triangular clusters with sizes of ∼2.2 nm.[64] When CO approaches monolayer coverage on Pt(557) at 1 Torr, the strong repulsion between CO molecules drives the Pt atoms away from steps, and therefore, causes the appearance of clusters. The CO gas pressure plays a crucial role: no clusters form at 10^{-7} Torr of CO; instead, the terrace widths and the step heights are doubled.

In the presence of O_2, Pt(557) undergoes a completely different morphologic restructuring process. An overlayer of clusters of approximately 1 nm in diameter cover the Pt(557) surface under a two-hour exposure to O_2.[65] These clusters were identified as surface Pt oxide by APXPS, which indicates an oxidation state change accompanying the morphology change (this was also the case for Pt(110)).[66] As a result, high-pressure STM studies on the stepped metal single crystals provide valuable information regarding the surface structure and morphology changes at low-coordinated sites. This information is critical in understanding the performance of real NP catalysts.

For bi- and multi- metallic NP catalysts, the particle architecture becomes increasingly complex,[67] and geometric arrangement of atoms on the surface (i.e., surface ensemble) becomes an important factor. In general, particle architecture impacts surface reactivity via geometric (i.e., ensemble) and/or electronic (i.e., "ligand") effects. Although a thorough and independent assessment of surface "ensemble" and "ligand" effects are difficult to make, the elemental composition on the immediate surface and in the near surface regions can be measured and correlated to surface activity and selectivity of heterogeneous catalytic reactions. By employing in situ surface techniques, we have recently applied this approach to model reactions in heterogeneous catalysis to address some of the most fundamental questions of surface reactivity.

2. Bimetallic Systems. (a). In Situ NEXAFS Spectroscopy Study of Correlation between Oxidized Co and the TOF of CO Oxidation Using Bimetallic CoPt NP Catalysts. A catalyst's susceptibility toward oxidation and reduction is another important metric for the efficacy of a catalyst. In situ NEXAFS was used to study the influence of Pt−Co alloy NPs.[68,69] In a reducing atmosphere of 1 bar H_2 at 250 °C, 4 nm Co NPs remain oxidized; whereas, 4 nm CoPt NPs were completely reduced at 1 bar H_2 and 125 °C. Figure 9 compares the

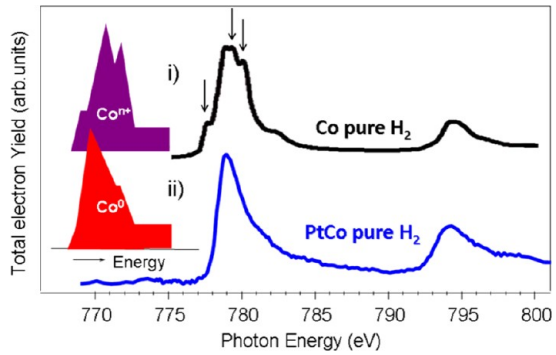

Figure 9. NEXAFS Co-L edge spectra of pure Co and bimetallic PtCo NP films under 1 bar H_2 and at 125 °C (reprinted with permission from ref 68, copyright 2011 American Chemical Society).

NEXAFS Co L-edge spectra of CoPt and Co, which were taken at Beamline 7.0.1 at the ALS. In a He atmosphere at room temperature, both Co and CoPt NPs are oxidized. The shoulders located above and below the main Co feature at 778.6 eV are characteristics of oxidized Co. Following reduction, the Co was reoxidized and the ratio of Co^0, Co^{2+}, and Co^{3+} was monitored. Reintroduction of 0.0048 Torr O_2 resulted in the preferential growth of Co^{2+} and the reduction of Co^0. As the pressure was increased to 36.2 Torr, Co^{3+} appears for both Co and CoPt; however, the Co NPs have a much larger oxidized fraction, whereby the Co^{3+} is formed at the expense of Co^{2+}.

In a follow-up NEXAFS study, the TOF of CO oxidation was found to directly correlate with the fraction of oxidized Co in CoPt NPs and the overall pressure of O_2:CO (Figure 10).[10] With an O_2:CO ratio of 1.4:1 and total pressures ranging from 0.01−100 Torr, the TOF increased by a factor of 10 (blue line - left axis) and the fraction of oxidized Co increased from zero to one (red line - right axis). Significantly, we found hysteresis for the Co oxidation state and TOF as the pressure was reduced.

dx.doi.org/10.1021/cs3004903 | ACS Catal. 2012, 2, 2250−2258

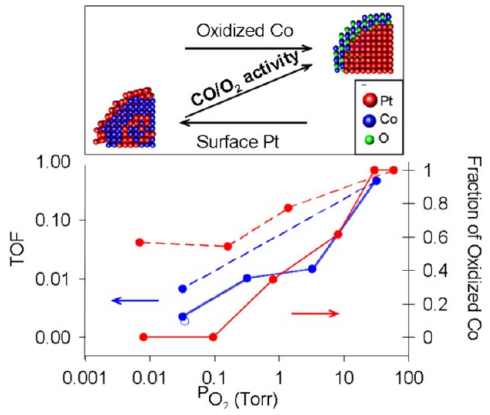

Figure 10. Turnover rates (left axis) and the fraction of oxidized Co^{n+} (right axis) as a function of O_2 partial pressures over the 4 nm PtCo NP films during the oxidation of CO. Depictions of the reaction-driven restructuring of bimetallic PtCo NPs (reprinted with permission from ref 69, copyright 2012 Elsevier).

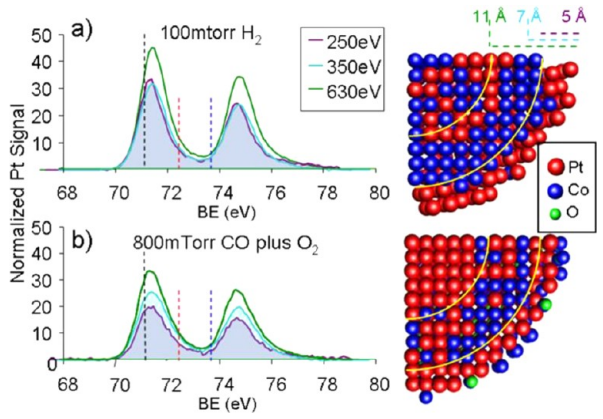

Figure 11. Normalized Pt 4f intensity at photon energies of 250, 350, and 630 eV that measure the composition of the 5, 7, and 11 Å topmost surface, respectively, under 100 mTorr H_2 (top) and 800 mTorr $CO+O_2$ (bottom) and at 125 °C. Illustrations of a 1/4 cross-section of a model spherical cluster based on the APXPS spectra. Pt atoms are shown in red, Co in blue and O in green (reprinted with permission from ref 69, copyright 2012 Elsevier).

This suggests that the $CO:O_2$ atmosphere induces a stable oxide phase concomitant with a phase segregation of the active Co oxide to the surface (as discussed in Elemental Composition section). These results indicate that the presence of oxidized Co controls the activity of oxidation reactions.

(b). APXPS Study of Bifunctional Catalysis Coupled to Oxide Chemistry with Bimetallic CoPt NP Catalysts. Oxyphilic metals incorporated into bimetallic alloy NPs invoke a bifunctional reaction mechanism,[70] where metal and metal oxide components activate different reactants. This phenomenon has been explored with 4 nm bimetallic PtCo alloy particles that have 50:50 bulk compositions. Three different photon energies were used to probe different layers of surface and subsurface regions.[69]

Depth profile analysis was carried out at 125 °C with H_2 (reducing atmosphere) and a 2:5 CO/O_2 reaction environment (oxidizing atmosphere). In a 100 mTorr H_2 reaction environment the 6 Å deep surface regions were found to be Pt-rich, whereas subsurface regions below the 6 Å region were depleted of Pt. Under a net oxidizing CO/O_2 reaction atmosphere, however, Co segregated to surface and formed predominantly metallic Co at 100 mTorr total pressures and oxides at 800 mTorr total pressures (Figure 11). For the CO/O_2 reaction at low mTorr partial pressures, pre-reduced alloy catalysts with Pt-rich surfaces were less active than the recycled catalyst with CoO_x rich surfaces. The behavior indicates that CoO_x coupled with Pt enhance reaction turnover (Figure 10).

(c). E-TEM Investigation of Bimetallic CoPt NP Catalysts under Reducing Gas Atmospheres. PtCo NPs of 11 nm diameter were also studied using E-TEM.[71] As-synthesized NPs measured in UHV conditions at 22 °C feature alloy architectures with random homogeneous distributions of individual atoms (Figure 12a). Under 100 mTorr H_2 and 250 °C, Pt segregates to surface regions and Co enriches the subsurface regions. Ex situ bright field (Figure 12b) and in situ dark field (Figures 12c and d) studies of smaller 4 nm CoPt NPs show corroborating evidence of the segregation. For the CO_2/H_2 reaction at 250 °C, with a 3:1 excess of H_2 at 5.5 bar, bimetallic PtCo NPs supported in mesoporous silica behaved Pt-like and produced CO with 99.9% selectivity via partial reduction of CO_2. However, under identical reaction conditions 10 nm pure Co NPs produced 30% CH_4.

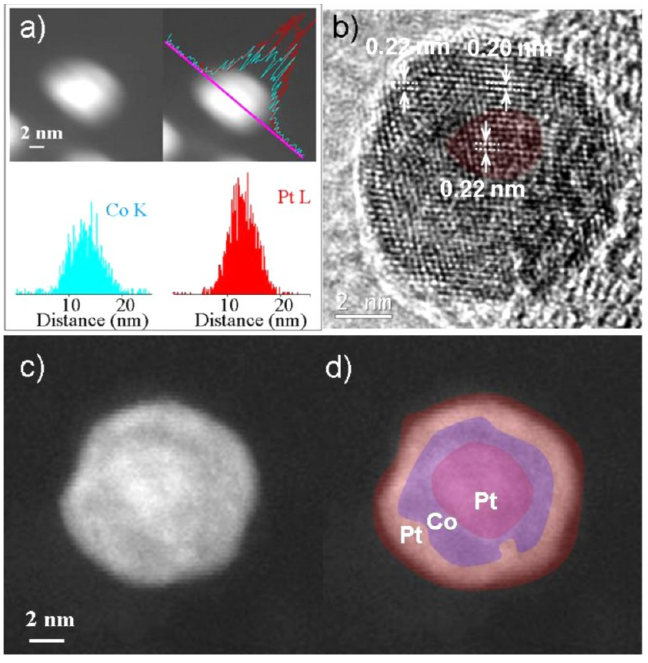

Figure 12. (a) Annular dark field image and STEM/EDS linescan at the Pt-L (red) and Co−K (blue) edges, and (b) bright field image taken under UHV. (c) E-TEM annular dark field images taken under 100 mTorr H_2 and at 250 °C, unprocessed and processed with color-codes, bright band on the surface and spot in the core, and (d) dark band in the subsurface, indicating Pt enrichment (red) and depletion (blue), respectively, in these regions (reprinted with permission from ref 71, copyright 2011 Springer).

■ CONCLUSIONS AND FUTURE DIRECTIONS

Well-defined model metal NP catalysts were studied in our lab by combining kinetic measurements with in situ surface spectroscopic and microscopic techniques operating under the identical conditions of catalytic reactions. Surface vibrational spectroscopy by SFG permits us to corroborate the results on the atomically clean surfaces of single crystals and (organic) capped NP surfaces under atmospheric pressures. While surface vibrational spectroscopy uncovers the steady-

dx.doi.org/10.1021/cs3004903 | ACS Catal. 2012, 2, 2250−2258

state surface structure, Synchrotron-based spectroscopic tools such as APXPS and in situ NEXAFS spectroscopy demonstrate that metal surfaces are dynamic in nature, and evolve to various equilibrium states as the catalytic reaction occurs. Hence, systematic in situ studies probing such surface dynamics are key to developing a universal understanding of the surface chemistry at the atomic and molecular levels in relation to heterogeneous catalysis.

Studies of catalysts under industrially relevant conditions are one of the major challenges in surface chemistry. Thus, continued development of instruments and experimental designs are an important task. Development of these tools for studies of solid−solid and solid−liquid interfaces will become more prevalent. For example solid−solid interfaces are present in multifunctional catalysts and in systems where metal−support interactions take place. Measurements of solid−liquid interfaces are important for understanding the heterogenizing of homogeneous catalysts and for energy applications such as lithium battery technologies and biological membranes.

AUTHOR INFORMATION

Corresponding Author

*E-mail: somorjai@berkeley.edu.

Funding

The work shown in this review article was supported by the Director, Office of Science, Office of Basic Energy Sciences, Division of Materials Sciences and Engineering of the U.S. Department of Energy under Contract No. DE-AC02-05cH11231.

Notes

The authors declare no competing financial interest.

REFERENCES

(1) Yin, Y.; Alivisatos, A. P. *Nature* **2005**, *437*, 664.
(2) An, K.; Alayoglu, S.; Ewers, T.; Somorjai, G. A. *J. Colloid Interface Sci.* **2012**, *373*, 1.
(3) Tao, F.; Grass, M. E.; Zhang, Y. W.; Butcher, D. R.; Renzas, J. R.; Liu, Z.; Chung, J. Y.; Mun, B. S.; Salmeron, M.; Somorjai, G. A. *Science* **2008**, *322*, 932.
(4) Tao, F.; Grass, M. E.; Zhang, Y. W.; Butcher, D. R.; Aksoy, F.; Aloni, S.; Altoe, V.; Alayoglu, S.; Renzas, J. R.; Tsung, C. K.; Zhu, Z. W.; Liu, Z.; Salmeron, M.; Somorjai, G. A. *J. Am. Chem. Soc.* **2010**, *132*, 8697.
(5) Rupprechter, G.; Freund, H. J. *Top. Catal.* **2001**, *14*, 3.
(6) Somorjai, G. A. *Catal. Lett.* **1992**, *12*, 17.
(7) Somorjai, G. A.; Vanhove, M. A. *Prog. Surf. Sci.* **1989**, *30*, 201.
(8) Weckhuysen, B. M. *Chem. Commun.* **2002**, 97.
(9) Tinnemans, S. J.; Mesu, J. G.; Kervinen, K.; Visser, T.; Nijhuis, T. A.; Beale, A. M.; Keller, D. E.; van der Eerden, A. M. J.; Weckhuysen, B. M. *Catal. Today* **2006**, *113*, 3.
(10) Barner, B. J.; Green, M. J.; Saez, E. I.; Corn, R. M. *Anal. Chem.* **1991**, *63*, 55.
(11) Shen, Y. R. *Nature* **1989**, *337*, 519.
(12) Baldelli, S.; Markovic, N.; Ross, P.; Shen, Y. R.; Somorjai, G. *J. Phys. Chem. B* **1999**, *103*, 8920.
(13) Su, X. C.; Cremer, P. S.; Shen, Y. R.; Somorjai, G. A. *J. Am. Chem. Soc.* **1997**, *119*, 3994.
(14) Su, X. C.; Cremer, P. S.; Shen, Y. R.; Somorjai, G. A. *Phys. Rev. Lett.* **1996**, *77*, 3858.
(15) Klunker, C.; Balden, M.; Lehwald, S.; Daum, W. *Surf. Sci.* **1996**, *360*, 104.
(16) Abbott, H. L.; Aumer, A.; Lei, Y.; Asokan, C.; Meyer, R. J.; Sterrer, M.; Shaikhutdinov, S.; Freund, H. J. *J. Phys. Chem. C* **2010**, *114*, 17099.
(17) Gao, F.; McClure, S. M.; Cai, Y.; Gath, K. K.; Wang, Y.; Chen, M. S.; Guo, Q. L.; Goodman, D. W. *Surf. Sci.* **2009**, *603*, 65.
(18) Rupprechter, G. *Advances in Catalysis*; Elsevier: New York, 2007; Vol. *51*, p 133.
(19) Shen, Y. R. *Surf. Sci.* **1994**, *299*, 551.
(20) Lambert, A. G.; Davies, P. B.; Neivandt, D. J. *Appl. Spectrosc. Rev.* **2005**, *40*, 103.
(21) Yang, M.; Somorjai, G. A. *J. Am. Chem. Soc.* **2004**, *126*, 7698.
(22) Ogletree, D. F.; Bluhm, H.; Lebedev, G.; Fadley, C. S.; Hussain, Z.; Salmeron, M. *Rev. Sci. Instrum.* **2002**, *73*, 3872.
(23) Grass, M. E.; Karlsson, P. G.; Aksoy, F.; Lundqvist, M.; Wannberg, B.; Mun, B. S.; Hussain, Z.; Liu, Z. *Rev. Sci. Instrum.* **2010**, *81*, 053106.
(24) Bart, J. C. J. *Adv. Catal.* **1986**, *34*, 203.
(25) Bottger, I.; Schedel-Niedrig, T.; Timpe, O.; Gottschall, R.; Havecker, M.; Ressler, T.; Schlogl, R. *Chem.—Eur. J.* **2000**, *6*, 1870.
(26) Akgul, G.; Aksoy, F.; Bozduman, A.; Ozkendir, O. M.; Ufuktepe, Y.; Luning, J. *Thin Solid Films* **2008**, *517*, 1000.
(27) Lytle, F. W.; Greegor, R. B.; Marques, E. C.; Biebesheimer, V. A.; Sandstrom, D. R.; Horsley, J. A.; Via, G. H.; Sinfelt, J. H. 1985, *288*, 280.
(28) Giorgio, S.; Joao, S. S.; Nitsche, S.; Chaudanson, D.; Sitja, G.; Henry, C. R. *Ultramicroscopy* **2006**, *106*, 503.
(29) Boyes, E. D.; Gai, P. L. *Ultramicroscopy* **1997**, *67*, 219.
(30) Wang, Z. L. *J. Phys. Chem. B* **2000**, *104*, 1153.
(31) Kung, K. Y.; Chen, P.; Wei, F.; Shen, Y. R.; Somorjai, G. A. *Surf. Sci.* **2000**, *463*, L627.
(32) Cremer, P. S.; Su, X. C.; Shen, Y. R.; Somorjai, G. A. *J. Am. Chem. Soc.* **1996**, *118*, 2942.
(33) Su, X. C.; Kung, K.; Lahtinen, J.; Shen, R. Y.; Somorjai, G. A. *Catal. Lett.* **1998**, *54*, 9.
(34) Su, X. C.; Kung, K. Y.; Lahtinen, J.; Shen, Y. R.; Somorjai, G. A. *J. Mol. Catal A: Chem.* **1999**, *141*, 9.
(35) McCrea, K. R.; Somorjai, G. A. *J. Mol. Catal A: Chem.* **2000**, *163*, 43.
(36) Yang, M.; Chou, K. C.; Somorjai, G. A. *J. Phys. Chem. B* **2003**, *107*, 5267.
(37) Bratlie, K. M.; Flores, L. D.; Somorjai, G. A. *Surf. Sci.* **2005**, *599*, 93.
(38) Somorjai, G. A.; Park, J. Y. *J. Chem. Phys.* **2008**, 128.
(39) Rioux, R. M.; Hsu, B. B.; Grass, M. E.; Song, H.; Somorjai, G. A. *Catal. Lett.* **2008**, *126*, 10.
(40) Wenyu, H.; Kuhn, J. N.; Chia-Kuang, T.; Yawen, Z.; Habas, S. E.; Peidong, Y.; Somorjai, G. A. *Nano Lett.* **2008**, 2027.
(41) Aliaga, C.; Tsung, C. K.; Alayoglu, S.; Komvopoulos, K.; Yang, P. D.; Somorjai, G. A. *J. Phys. Chem. C* **2011**, *115*, 8104.
(42) Krier, J. M.; Michalak, W. D.; Baker, L. R.; An, K.; Komvopoulos, K.; Somorjai, G. A. *J. Phys. Chem. C* **2012**, *116* (33), 17540.
(43) Borodko, Y.; Humphrey, S. M.; Tilley, T. D.; Frei, H.; Somorjai, G. A. *J. Phys. Chem. C* **2007**, *111*, 6288.
(44) Kuhn, J. N.; Tsung, C. K.; Huang, W.; Somorjai, G. A. *J. Catal.* **2009**, *265*, 209.
(45) Zhang, Y. W.; Grass, M. E.; Kuhn, J. N.; Tao, F.; Habas, S. E.; Huang, W. Y.; Yang, P. D.; Somorjai, G. A. *J. Am. Chem. Soc.* **2008**, *130*, 5868.
(46) Kuhn, J. N.; Huang, W. Y.; Tsung, C. K.; Zhang, Y. W.; Somorjai, G. A. *J. Am. Chem. Soc.* **2008**, *130*, 14026.
(47) Rice, C. A.; Worley, S. D.; Curtis, C. W.; Guin, J. A.; Tarrer, A. R. *J. Chem. Phys.* **1981**, *74*, 6487.
(48) Kummer, J. T. *J. Phys. Chem.* **1986**, *90*, 4747.
(49) Carrette, L.; Friedrich, K. A.; Stimming, U. *Fuel Cells* **2001**, *1*, 5.
(50) Kitchin, J. R.; Norskov, J. K.; Barteau, M. A.; Chen, J. G. *Phys. Rev. Lett.* **2004**, *93* (15), 156801.
(51) Stamenkovic, V. R.; Mun, B. S.; Arenz, M.; Mayrhofer, K. J. J.; Lucas, C. A.; Wang, G. F.; Ross, P. N.; Markovic, N. M. *Nat. Mater.* **2007**, *6*, 241.
(52) Meier, D. C.; Goodman, D. W. *J. Am. Chem. Soc.* **2004**, *126*, 1892.

(53) Chen, M. S.; Cal, Y.; Yan, Z.; Gath, K. K.; Axnanda, S.; Goodman, D. W. *Surf. Sci.* **2007**, *601*, 5326.
(54) Kleis, J.; Greeley, J.; Romero, N. A.; Morozov, V. A.; Falsig, H.; Larsen, A. H.; Lu, J.; Mortensen, J. J.; Dulak, M.; Thygesen, K. S.; Norskov, J. K. *Chem. Abstr.* **2011**, *242*.
(55) Meier, J.; Schiotz, J.; Liu, P.; Norskov, J. K.; Stimming, U. *Chem. Phys. Lett.* **2004**, *390*, 440.
(56) Molenbroek, A. M.; Norskov, J. K.; Clausen, B. S. *J. Phys. Chem. B* **2001**, *105*, 5450.
(57) Tang, W.; Peterson, A. A.; Varela, A. S.; Jovanov, Z. P.; Bech, L.; Durand, W. J.; Dahl, S.; Norskov, J. K.; Chorkendorff, I. *Phys. Chem. Chem. Phys.* **2012**, *14*, 76.
(58) Vajda, S.; Pellin, M. J.; Greeley, J. P.; Marshall, C. L.; Curtiss, L. A.; Ballentine, G. A.; Elam, J. W.; Catillon-Mucherie, S.; Redfern, P. C.; Mehmood, F.; Zapol, P. *Nat. Mater.* **2009**, *8*, 213.
(59) Li, Y. M.; Liu, J. H. C.; Witham, C. A.; Huang, W. Y.; Marcus, M. A.; Fakra, S. C.; Alayoglu, P.; Zhu, Z. W.; Thompson, C. M.; Arjun, A.; Lee, K.; Gross, E.; Toste, F. D.; Somorjai, G. A. *J. Am. Chem. Soc.* **2011**, *133*, 13527.
(60) Witham, C. A.; Huang, W. Y.; Tsung, C. K.; Kuhn, J. N.; Somorjai, G. A.; Toste, F. D. *Nat. Chem.* **2010**, *2*, 36.
(61) Grass, M. E.; Zhang, Y. W.; Butcher, D. R.; Park, J. Y.; Li, Y. M.; Bluhm, H.; Bratlie, K. M.; Zhang, T. F.; Somorjai, G. A. *Angew. Chem., Int. Ed.* **2008**, *47*, 8893.
(62) Mcintyre, B. J.; Salmeron, M.; Somorjai, G. A. *J. Vac. Sci. Technol. A* **1993**, *11*, 1964.
(63) Tao, F.; Tang, D.; Salmeron, M.; Somorjai, G. A. *Rev. Sci. Instrum.* **2008**, *79*, 084101.
(64) Tao, F.; Dag, S.; Wang, L. W.; Liu, Z.; Butcher, D. R.; Bluhm, H.; Salmeron, M.; Somorjai, G. A. *Science* **2010**, *327*, 850.
(65) Zhu, Z. W.; Tao, F.; Zheng, F.; Chang, R.; Li, Y. M.; Heinke, L.; Liu, Z.; Salmeron, M.; Somorjai, G. A. *Nano Lett.* **2012**, *12*, 1491.
(66) Butcher, D. R.; Grass, M. E.; Zeng, Z. H.; Aksoy, F.; Bluhm, H.; Li, W. X.; Mun, B. S.; Somorjai, G. A.; Liu, Z. *J. Am. Chem. Soc.* **2011**, *133*, 20319.
(67) Hwang, B. J.; Sarma, L. S.; Chen, J. M.; Chen, C. H.; Shih, S. C.; Wang, G. R.; Liu, D. G.; Lee, J. F.; Tang, M. T. *J. Am. Chem. Soc.* **2005**, *127*, 11140.
(68) Zheng, F.; Alayoglu, S.; Guo, J. H.; Pushkarev, V.; Li, Y. M.; Glans, P. A.; Chen, J. L.; Somorjai, G. *Nano Lett.* **2011**, *11*, 847.
(69) Zheng, F.; Alayoglu, S.; Pushkarev, V. V.; Beaumont, S. K.; Specht, C.; Aksoy, F.; Liu, Z.; Guo, J. H.; Somorjai, G. A. *Catal. Today* **2012**, *182*, 54.
(70) Bunluesin, T.; Gorte, R. J.; Graham, G. W. *Appl. Catal., B* **1998**, *15*, 107.
(71) Alayoglu, S.; Beaumont, S. K.; Zheng, F.; Pushkarev, V. V.; Zheng, H. M.; Iablokov, V.; Liu, Z.; Guo, J. H.; Kruse, N.; Somorjai, G. A. *Top. Catal.* **2011**, *54*, 778.